International Journal of Computer Science & Communication (ISSN: 0973-7391)
Volume 12• Issue 1 pp. 38-49 Sept 2020 - March 2021 www.csjournals.com

Corrosion-resistant behavior of R F sputtered TiO_2 thin film on Aluminium substrate at different temperatures

Udit Gupta[a], Kailash Pandey[b], Rakesh Jain[a]*, Rajeev Gupta

[a]Department of Physics, Shobhit Institute of Engineering & Technology, Meerut- 250110 Uttar Pradesh, India
[b]Department of Physics, School of Engineering Studies, University of Petroleum & Energy Studies, Dehradun-248007, Uttarakhand, India

Abstract: A study was conducted to improve the hydrophobicity and corrosion resistance behavior of Al6061 using RF-sputtered TiO_2 thin film at various temperatures. In this experiment, the surface properties were correlated with the coating process. Using a goniometer, we determined the wettability of the surfaces. Salt spray corrosion tests were performed to evaluate topographical changes. X-ray diffraction (XRD) and Contact Angle Goniometer techniques were used to characterize the deposited coatings. Comparing the TiO_2 coating applied at 400°C with that applied at other temperatures, showed the highest water contact angle. In an industrial application, TiO_2 coatings with hydrophobic properties delay corrosion at 400°C, resulting in durability.

Keywords: Aluminium substrate; corrosion, RF-sputtering; TiO_2 coating, Contact Angle, wettability

1 Introduction:

Aluminum alloy Al6061 is widely used in industry and at home because of several benefits over pure metals, like better corrosion resistance, lower costs, higher strength, and better workability, machinability, ductility, and brittleness[1]. In multiple industries, it is preferred because of its outstanding strength, good corrosion resistance, and good machinability. As a result of its remarkable strength and lightweight properties, it is a perfect choice for endeavors that seek to reduce weight and increase durability[2]. A protective oxide layer forms on Al6061 when exposed to oxygen, which makes it moderately corrosion resistant[3]. As a result, the underlying metal is protected from further oxidation. Despite harsh environmental conditions, Al6061 components maintain their durability and longevity[4]. Hydrophobic properties are not naturally

present in Al6061 aluminum alloy when left untreated. Hydrophobic surfaces offer advantages such as repelling liquids, preventing the adhesion of biological substances like proteins and cells to medical devices and implants, reducing water absorption, maintaining dryness, self-cleaning capabilities, improving corrosion resistance, reducing ice formation, and enhancing biomedical applications[5]. The corrosion, icing, and self-cleaning properties of hydrophobic surfaces would be advantageous for Al6061 alloy applications[6]. Aluminum surfaces are generally hydrophilic, meaning water droplets naturally adhere to and spread out. Thus, Al6061 alloy could be made more useful by creating a hydrophobic surface[7]. The surface topography can be modified, or a superficial layer of a hydrophobic compound can be deposited to make a hydrophobic surface[8]. The chemical modification of surfaces is a standard method for creating hydrophobic surfaces. Additionally, surface roughening can alter the surface topology by forming micro or nano-patterns or by deposition of nanoparticles, which can significantly enhance the hydrophobicity of materials[9], [10].

Due to its exceptional heat resistance properties, titanium dioxide (TiO_2) is widely employed in various applications, including fuel cells, solar cells, and sensors. The self-cleaning properties of TiO_2 coatings enhance the performance of the materials beneath them, and they can also be applied to enhance the performance[11], [12], [13]. Its biocompatibility and antibacterial properties also make TiO_2 ideal for medical applications. Surfaces with hydrophobic properties can be developed using TiO_2[14], [15], [16]. Surface energy can be decreased in various ways, including altering the electronic structure, creating surface defects and vacancies, making the surface rougher, and reducing water adsorption[17]. It involves atomized material deposition in a vacuum environment and is a technique used for vaporization coatings. With radiofrequency (RF) sputtering, film composition can be controlled more easily; deposition rates can be increased, substrate temperatures can be kept low, film coverage is uniform, adhesion and density are enhanced, reactive sputtering can be performed, and scalability can be achieved[18], [19], [20].

RF sputtering enhances the hydrophobicity of thin film coatings like TiO_2 when combined with surface roughening techniques on substrates like Al6061. There are several techniques documented in the literature for creating surface roughness on coatings. The RF-sputtering parameters of RF-sputtered TiO_2 particles were varied on Al6061 steel surfaces in this study to

fulfill the above objective[21], [22]. In addition to contact angle goniometers, X-ray diffractions, configured samples were characterized. Water jets were used at various heights to assess mechanical stability. Water contact angles were also measured using the sessile drop method to assess the samples' hydrophobicity. Last, salt spray testing was conducted to determine whether TiO_2 coatings are corrosion resistant.

2 Experimentation

2.1 Materials

Al6061 aluminum alloy was the substrate material [contains 1.1% magnesium, 0.14 wt% manganese, 0.46 wt% silicon, 0.16 wt% iron, and 98.11 wt% aluminum]. The acquired alloy was sectioned into specimen pieces measuring 15 x 15 mm^2 using wire electrode discharge machining to avoid any microstructural transformations. A flat reference surface was achieved to remove surface oxides using different emery paper grades. Distilled water and ethanol were used to clean any remaining debris from the polished samples, and to remove any remaining debris from them, ultrasonic cleaning was performed.

2.2 RF- Magnetron Sputtering

The polished Al6061 alloy surface were used to deposit TiO_2 coating by using RF sputtering with different temperatures. Turbo-molecular pumps were used to evacuate the working chamber thoroughly to $6.1x10^{-6}$ mbar[23], [24]. It was possible to conduct the trials in a clean, controlled environment after the area was evacuated. The surface of the target material was further cleaned during the penniform sputtering stage, which lasted for five minutes. As a result of this pre-sputtering process, any remaining impurities on the target surface were successfully removed. After the sputtering phase, the primary sputtering process began, and deposition took 90 minutes. We used 100W of power for the RF sputtering process. RF sputtering achieves substantial coating thicknesses for TiO_2 only at 300°C and above.

Furthermore, the gas flow rate was 30 standard cubic centimeters per minute (sccm) and the sputtering pressure was 3×10^{-2} mbar. A constant rotational speed of 10 RPM was used to maintain a uniform coating thickness. These parameters were carefully selected and regulated for homogeneous deposition of TiO_2 on Al6061 substrates. These macro images illustrate the

sputtered Al6061 and RF magnetron coating specimens, Target TiO_2 Temperature (°C) 300 400 500 Base Pressure (mbar) 6.1×10^(-6) Pre-sputtering (min) 5 Sputtering Pressure (mbar) 3×10^(-2) Power (W) 100 Sputtering time (90) 90 Gas Argon Flow rate 30 sccm Rotation (RPM) 10 A TiO_2 coated; A+ TiO_2 coated.

2.3 Thin-Film Characterization

2.3.1 Water Contact Angle

We used a goniometer with microlens and a CCD camera to measure the surface's water contact angle (WCA) under investigation. DSA 25, Kruss, drop shape analyzer device with a high accuracy of about 0.05° was used. We carefully deposited a 10µL water microdroplet onto the surface to determine the WCA using the sessile drop method. To achieve this, a syringe was connected to a goniometer to allow precise placement of droplets. Analysis and evaluation of the shape of the water droplet were enabled the calculation of the static contact angle. Three separate locations were chosen to ensure the accuracy of WCA measurements.

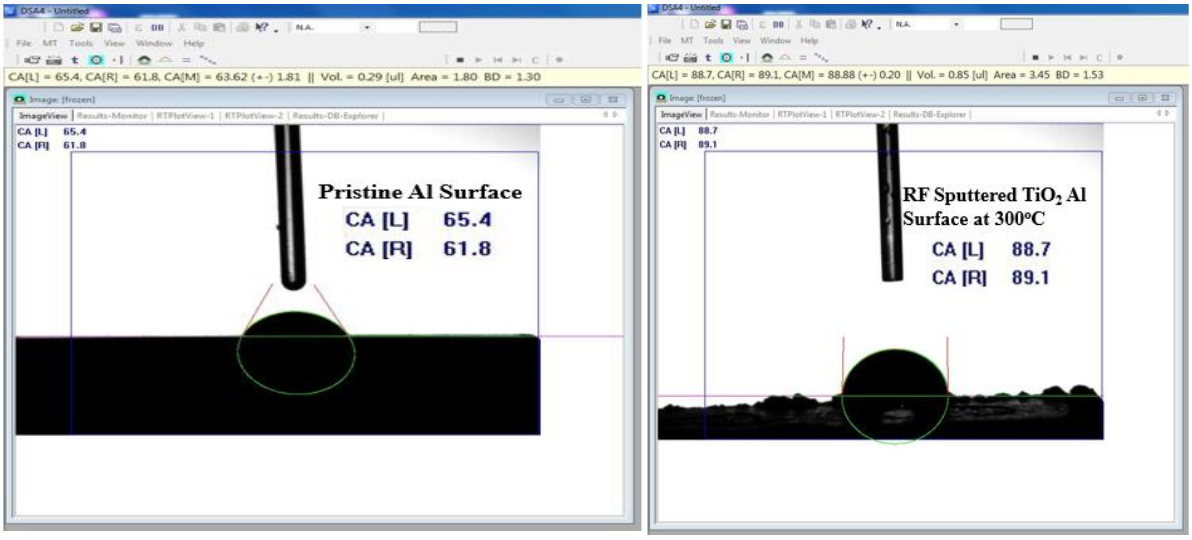

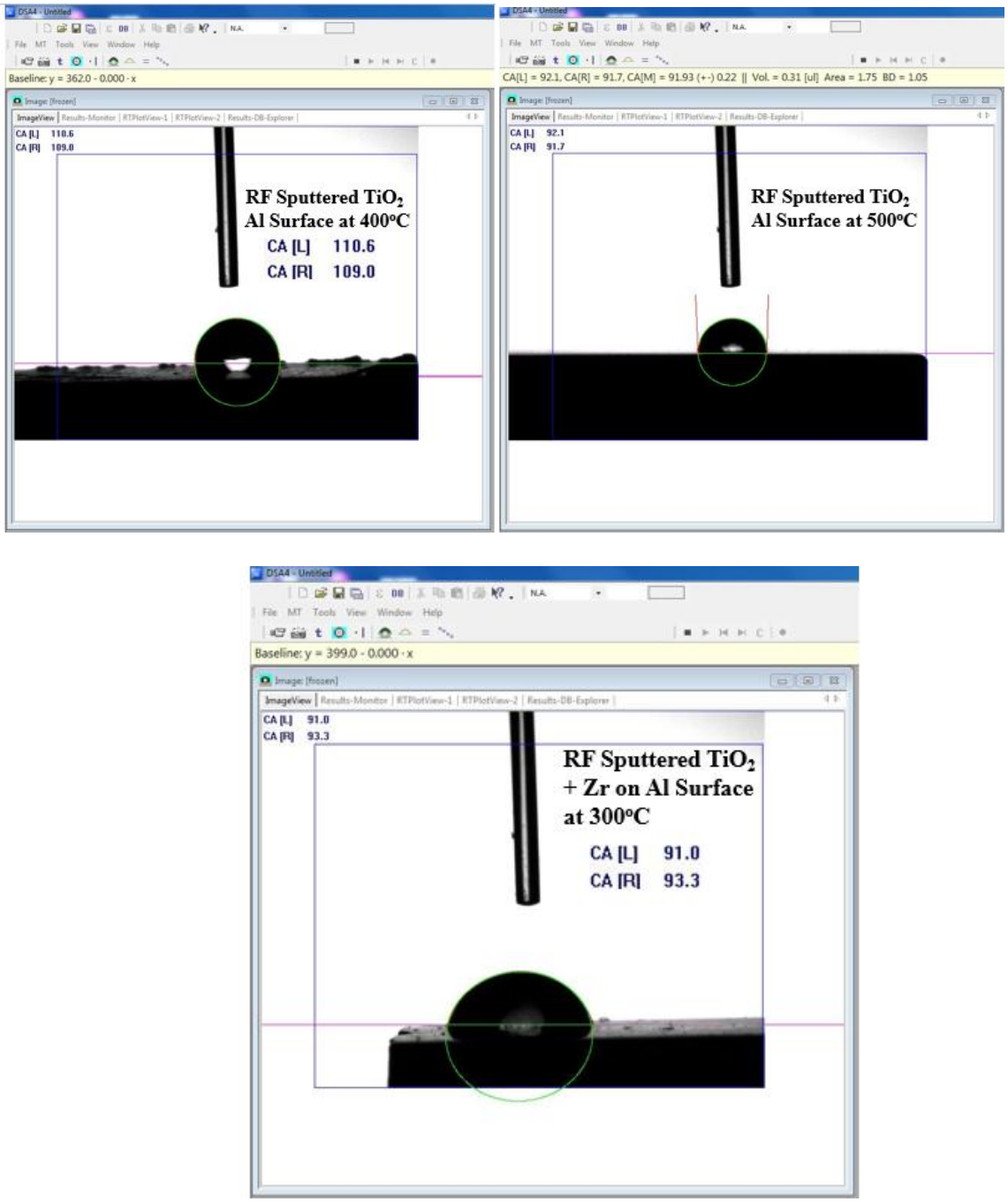

Figure 1:The wettability test through contact angle of pristine and RF sputtered TiO_2 coating on Al substrate with different temperatures 300^{o}C, 400^{o} C, 500^{o}C and at 300^{o}C, TiO_2 +Zr

These individual measurements were averaged to report the WCA of the surface. The contact angle for pristine Al surface was 63.6^{o} (avg.), and the contact angle value increases on RF sputtered TiO_2 film. At 300^{o}C, the contact angle is 88.9^{o}, and its value reaches its maximum

value of approx. 110^{o} at 400^{o} C. This increase in contact angle may be due to the formation of a rough structure of TiO_2 on Al surface. Further, at 500^{o}C, its value decreases. It may fill gaps with a grain of titania, making the surface smoother. The higher the contact angle, the lower the wettability, i.e., the wettability of corrosive molecules. This gives very little interaction between coating and corrosive molecules, resulting in very little corrosion[23], [24] [Fig 2].

2.3.2 Surface Characterization

The grown TiO_2 samples underwent a comprehensive characterization process to investigate their structural and morphological properties under different surface treatment conditions. The development of compounds and their phase structure was ascertained through XRD analysis covering a diffraction angle (2θ) range from 15° to 80°[25], [26]. The XRD data were obtained using PANalytical Empyrean XRD equipment with a Cu anode and K-α radiation (wavelength of 1.54060 Å) at 40 mA and 45 KV. The Full Width at Half Maximum (FWHM) was used for peak analysis with a precise step size of 0.0170 and 30 minutes of scanning time to ensure sufficient data points. The average crystal size of the coated surface was calculated using the Scherrer methodology, which considers the diffraction patterns from various lattice planes, each having a different crystal size.

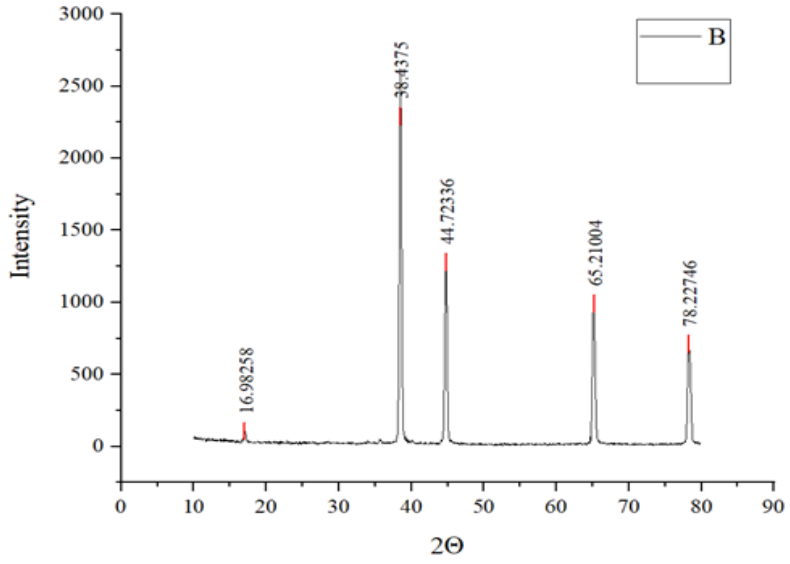

Figure 2: XRD pattern of RF sputtered TiO2 coated Al at 400^{O} C

This analysis allowed us to determine the average crystal size of the particles on the coated surface. Additionally, the dislocation density of the particles on the surface of the coating was quantified, providing insights into defects within the crystal structure of the coated surface. The micro-strains of the coated surface were also evaluated. Micro-strain refers to the small atomic distortions and deformations occurring around dislocation lines due to the presence of extra planes of atoms. This measurement provides information about the strain on the coated surface resulting from these atomic distortions[27], [28].

To assess the mechanical behaviour and stability of the coating, the uniform strain density function was used to calculate the stress developed on the coating surface [31-32]. The crystallinity of the coated surface was determined by analyzing the peaks in the XRD pattern. Crystallinity was quantified by considering the area under the peaks and comparing it to the total area of all the peaks in the XRD pattern. By conducting this comprehensive analysis of XRD data, including crystal size, dislocation density, micro-strain, stress, and crystallinity, a thorough understanding of the structural characteristics and properties of the coated surface was achieved.

Closer inspection reveals that carbon deposition on the specimen's surface was somewhat greater than that of titanium and oxygen. The carbon deposition on the surface of the substrate indicates some intrude reactions taking place during the RF sputtering coating. However, the successful deposition of titanium and oxygen particles on the specimen surface confirms the effectiveness of the RF sputtering technique in achieving the desired coating. The acquired peak positions (2Θ), Full-width at half maximum (FWHM - β), and the corresponding hkl miller indices were employed to determine the crystallographic characteristics (Figure 2). The lattice parameters a=9.769 Å, b=2.921 Å, and c=4.675 Å were used to determine the orthorhombic crystal structure of the TiO_2 particles. The XRD pattern in Figure 2 illustrates that the sputtered film at 300°C had a lower degree of crystallinity, or smaller crystal grains were observed as indicated by the strength of peaks. This is also indicated by the crystal size shown in Figure 2 . As the sputtering temperature increased to 400°C and 500°C, the crystallinity of grains improved, potentially resulting in larger and more well-defined crystal structures.

2.3.3 Salt-Spray Corrosion Study

A corrosion study was conducted on the coated and uncoated surfaces to assess the effectiveness of the reported coating in protecting the underlying substrate from corrosion. In this study, salt spray corrosion testing was employed to evaluate the corrosion resistance of the reported surface. With practical application in mind, this test subjected the coated surfaces to a highly corrosive environment (3.5% NaCl) for 52 hours, accelerating the corrosion process and assessing the protective capabilities. Visual inspection of the coated and uncoated specimens was done at regular intervals of 8 hours during the salt-spray cyclic test. The bare aluminum specimen turned blackish after 8 hours of the test, which turned greyish and later dull white after seven cycles of testing. During the test, the specimen showed high corrosion, and the products kept leaving the surface. A pale rusty red colour was observed on the coated surface, with low signs of corrosion products forming on the coated TiO_2 surface. Following 52 hours of salt spray testing, the surface contained corrosion products. An ultrasonic cleaning procedure was employed to remove loose particles resulting from oxidative corrosion to visualize the surface underneath. Subsequently, the specimens were dried for 20 minutes at 50°C to eliminate any remaining moisture. The pristine aluminum exhibited excessive pitting marks and oxidation signs because of continuing contact in a corrosive environment. Surface morphology indicates the formation of an oxide layer due to salt water reaction with aluminum. The growing Al_2O_3 layer with the exposure time is believed to passivate the further corrosion of the underlying surface. The galvanic cell that develops during corrosion involves the formation of pits acting as the anode, with the metal serving as the cathode. This setup leads to the migration of anions towards the pits and consequently results in the localized production of metal cations. The aluminum cations create an excessive positive charge while attracting chlorine ions, forming the Al_2O_3, which reacts with water molecules in a moist test chamber to form hydrogen gas. The film-breaking mechanism caused by pitting corrosion causes the continual detachment of the oxide film to form. The coated specimen exhibited much less corrosion, and the polishing marks were visible. However, some trivial oxidation clusters were visible, and the specimen surface was free from any major pitting marks. The delay in corrosion of the aluminum substrate indicates the effectiveness of TiO_2 coating for corrosion protection against hostile saline environments.

Since the specimens were not masked, the increase in Al may be its diffusion from the substrate side to the surface during the corrosion testing. 52 hours of prolonged oxidation later led to cracks in the oxide clusters due to the thermal coefficient mismatch experienced during the corrosion cycles. While comparing the EDS elemental composition of the salt-sprayed specimen to the chemical boiled, it may be noticed that the elements were retained in a larger proportion. However, a lesser amount of O and Al is present, indicating lesser oxidation in the boiled specimen. This augmentation enhances the surface's air-trapping capacity, improving non-wetting behavior compared to TiO_2 coating. Additionally, the chemical composition analysis of the reported corroded surface through line scanning reveals an increase in the percentage of oxide layer. This is attributed to oxide formation during salt spray testing, with the foam-like structure formed during chemical etching playing a crucial role in trapping these oxides.

3 Conclusion

The study aimed to improve the hydrophobic behavior and corrosion resistance of the Al6061 substrate by deposition of coatings using RF-sputtering at various temperatures. The following conclusions have been summarized, surface roughness and surface profile were notably influenced by the sputtering temperature. Higher temperatures resulted in a more distinct crystalline structure and reduced micro-strain within the coatings. This phenomenon was attributed to the enhanced mobility of adatoms during sputtering at 400°C. Initially, the TiO_2 coatings exhibited hydrophilic properties, but as the sputtering temperature increased, their behavior shifted towards hydrophobic due to an increase in surface roughness. Corrosion testing in a salt spray environment indicated that the TiO_2 coating exhibited improved corrosion resistance. Minimum corrosive damage was observed after 32 hours of exposure to a highly corrosive environment.

References:

[1] A. Kareem, J. A. Qudeiri, A. Abdudeen, T. Ahammed, and A. Ziout, “A Review on AA 6061 Metal Matrix Composites Produced by Stir Casting,” *Materials*, vol. 14, no. 1, pp. 1–22, Jan. 2021, doi: 10.3390/MA14010175.

[2] A. Kareem, J. A. Qudeiri, A. Abdudeen, T. Ahammed, and A. Ziout, “A Review on AA 6061 Metal Matrix Composites Produced by Stir Casting,” *Materials*, vol. 14, no. 1, pp. 1–22, Jan. 2021, doi: 10.3390/MA14010175.

[3] Y. M. Han and X. G. Chen, “Electrochemical Behavior of Al-B4C Metal Matrix Composites in NaCl Solution,” *Materials 2015, Vol. 8, Pages 6455-6470*, vol. 8, no. 9, pp. 6455–6470, Sep. 2015, doi: 10.3390/MA8095314.

[4] B. Mao, A. Siddaiah, Y. Liao, and P. L. Menezes, “Laser surface texturing and related techniques for enhancing tribological performance of engineering materials: A review,” *J Manuf Process*, vol. 53, pp. 153–173, May 2020, doi: 10.1016/J.JMAPRO.2020.02.009.

[5] E. J. Falde, S. T. Yohe, Y. L. Colson, and M. W. Grinstaff, “Superhydrophobic Materials for Biomedical Applications,” *Biomaterials*, vol. 104, p. 87, Oct. 2016, doi: 10.1016/J.BIOMATERIALS.2016.06.050.

[6] V. K. Sharma, V. Kumar, and R. S. Joshi, “Manufacturing of stable hydrophobic surface on rare-earth oxides aluminium hybrid composite,” *https://doi.org/10.1177/0954408920979105*, vol. 235, no. 4, pp. 899–912, Dec. 2020, doi: 10.1177/0954408920979105.

[7] M. A. M. Ali, A. I. Azmi, M. N. Murad, M. Z. M. Zain, A. N. M. Khalil, and N. A. Shuaib, “Roles of new bio-based nanolubricants towards eco-friendly and improved machinability of Inconel 718 alloys,” *Tribol Int*, vol. 144, p. 106106, Apr. 2020, doi: 10.1016/J.TRIBOINT.2019.106106.

[8] P. Dimitrakellis and E. Gogolides, “Hydrophobic and superhydrophobic surfaces fabricated using atmospheric pressure cold plasma technology: A review,” *Adv Colloid Interface Sci*, vol. 254, pp. 1–21, Apr. 2018, doi: 10.1016/J.CIS.2018.03.009.

[9] A. O. Ijaola *et al.*, “Wettability Transition for Laser Textured Surfaces: A Comprehensive Review,” *Surfaces and Interfaces*, vol. 21, p. 100802, Dec. 2020, doi: 10.1016/J.SURFIN.2020.100802.

[10] A. R. Esmaeili, N. Mir, and R. Mohammadi, “A facile, fast, and low-cost method for fabrication of micro/nano-textured superhydrophobic surfaces,” *J Colloid Interface Sci*, vol. 573, pp. 317–327, Aug. 2020, doi: 10.1016/J.JCIS.2020.04.027.

[11] A. Afzal, A. Habib, I. Ulhasan, M. Shahid, and A. Rehman, “Antireflective Self-Cleaning TiO2 Coatings for Solar Energy Harvesting Applications,” *Front Mater*, vol. 8, p. 687059, Jun. 2021, doi: 10.3389/FMATS.2021.687059/BIBTEX.

[12] X. Kang, S. Liu, Z. Dai, Y. He, X. Song, and Z. Tan, “Titanium Dioxide: From Engineering to Applications,” *Catalysts 2019, Vol. 9, Page 191*, vol. 9, no. 2, p. 191, Feb. 2019, doi: 10.3390/CATAL9020191.

[13] N. Kaur, M. Singh, A. Moumen, G. Duina, and E. Comini, “1D Titanium Dioxide: Achievements in Chemical Sensing,” *Materials*, vol. 13, no. 13, pp. 1–21, Jul. 2020, doi: 10.3390/MA13132974.

[14] S. Jafari, B. Mahyad, H. Hashemzadeh, S. Janfaza, T. Gholikhani, and L. Tayebi, “Biomedical applications of TiO2 nanostructures: Recent advances,” *Int J Nanomedicine*, vol. 15, pp. 3447–3470, 2020, doi: 10.2147/IJN.S249441.

[15] V. Kumaravel *et al.*, “Antimicrobial TiO2 nanocomposite coatings for surfaces, dental and orthopaedic implants,” *Chemical Engineering Journal*, vol. 416, p. 129071, Jul. 2021, doi: 10.1016/J.CEJ.2021.129071.

[16] N. T. Padmanabhan and H. John, “Titanium dioxide based self-cleaning smart surfaces: A short review,” *J Environ Chem Eng*, vol. 8, no. 5, p. 104211, Oct. 2020, doi: 10.1016/J.JECE.2020.104211.

[17] A. Badreldin, A. E. Abusrafa, and A. Abdel-Wahab, “Oxygen-Deficient Cobalt-Based Oxides for Electrocatalytic Water Splitting,” *ChemSusChem*, vol. 14, no. 1, pp. 10–32, Jan. 2021, doi: 10.1002/CSSC.202002002.

[18] G. Mahendra *et al.*, “RF Sputter-Deposited Nanostructured CuO Films for Micro-Supercapacitors,” *Applied Nano 2021, Vol. 2, Pages 46-66*, vol. 2, no. 1, pp. 46–66, Feb. 2021, doi: 10.3390/APPLNANO2010005.

[19] J. Daughtry, A. S. Alotabi, L. Howard-Fabretto, and G. G. Andersson, “Composition and properties of RF-sputter deposited titanium dioxide thin films,” *Nanoscale Adv*, vol. 3, no. 4, p. 1077, Feb. 2021, doi: 10.1039/D0NA00861C.

[20] N. K. Das *et al.*, “Effect of substrate temperature on the properties of RF sputtered CdS thin films for solar cell applications,” *Results Phys*, vol. 17, p. 103132, Jun. 2020, doi: 10.1016/J.RINP.2020.103132.

[21] J. Daughtry, A. S. Alotabi, L. Howard-Fabretto, and G. G. Andersson, "Composition and properties of RF-sputter deposited titanium dioxide thin films," *Nanoscale Adv*, vol. 3, no. 4, p. 1077, Feb. 2021, doi: 10.1039/D0NA00861C.

[22] O. G. Simionescu, C. Romanitan, O. Tutunaru, V. Ion, O. Buiu, and A. Avram, "RF Magnetron Sputtering Deposition of TiO2 Thin Films in a Small Continuous Oxygen Flow Rate," *Coatings 2019, Vol. 9, Page 442*, vol. 9, no. 7, p. 442, Jul. 2019, doi: 10.3390/COATINGS9070442.

[23] S. Noormohammed and D. K. Sarkar, "Rf-Sputtered Teflon®-Modified Superhydrophobic Nanostructured Titanium Dioxide Coating on Aluminum Alloy for Icephobic Applications," *Coatings 2021, Vol. 11, Page 432*, vol. 11, no. 4, p. 432, Apr. 2021, doi: 10.3390/COATINGS11040432.

[24] J. Daughtry, A. S. Alotabi, L. Howard-Fabretto, and G. G. Andersson, "Composition and properties of RF-sputter deposited titanium dioxide thin films," *Nanoscale Adv*, vol. 3, no. 4, p. 1077, Feb. 2021, doi: 10.1039/D0NA00861C.

[25] T. Theivasanthi and M. Alagar, "Titanium dioxide (TiO 2) Nanoparticles-XRD Analyses-An Insight".

[26] J. Wei, B. Li, L. Jing, N. Tian, X. Zhao, and J. Zhang, "Efficient protection of Mg alloy enabled by combination of a conventional anti-corrosion coating and a superamphiphobic coating," *Chemical Engineering Journal*, vol. 390, p. 124522, Jun. 2020, doi: 10.1016/J.CEJ.2020.124522.

[27] A. M. Alsaad *et al.*, "Optical, Structural, and Crystal Defects Characterizations of Dip Synthesized (Fe-Ni) Co-Doped ZnO Thin Films," *Materials 2020, Vol. 13, Page 1737*, vol. 13, no. 7, p. 1737, Apr. 2020, doi: 10.3390/MA13071737.

[28] K. V. Chandekar and K. M. Kant, "Size-strain analysis and elastic properties of CoFe2O4 nanoplatelets by hydrothermal method," *J Mol Struct*, vol. 1154, pp. 418–427, Feb. 2018, doi: 10.1016/J.MOLSTRUC.2017.09.104.